International Journal of Minerals, Metallurgy and Materials
Volume 22, Number 4, April 2015, Page 371
DOI: 10.1007/s12613-015-1082-2

Optimized use of MgO flux in the agglomeration of high-chromium vanadium–titanium magnetite

Jue Tang, Man-sheng Chu, and Xiang-xin Xue

School of Material and Metallurgy, Northeastern University, Shenyang 110819, China
(Received: 25 March 2014; revised: 12 May 2014; accepted: 13 May 2014)

Abstract: The optimized use of MgO flux in the agglomeration of high-chromium vanadium–titanium magnetite was investigated systematically through sinter and pellet experiments. MgO was added in the form of magnesite. When the content of MgO in the sinter was increased from 1.95wt% to 2.63wt%, the low-temperature reduction degradation index increased from 80.57% to 82.71%. When the content of MgO in the pellet was increased from 1.14wt% to 2.40wt%, the reduction swelling index decreased from 15.2% to 8.6%; however, the compressive strength of the oxidized pellet decreased dramatically and it was 1985 N with an MgO content of 1.14wt%. This compressive strength does not satisfy the requirements for blast-furnace production. When all of the aforementioned results were taken into account, the sinter with a high MgO content (2.63wt%) matching the pellet with a low MgO content (less than 1.14wt%) was the rational burden structure for smelting high-chromium vanadium–titanium magnetite in blast furnaces.

Keywords: magnetite; ore pellets; magnesia; agglomeration; burden; sintering

1. Introduction

Modern blast furnace (BF) essentially needs most of the iron-bearing burden to be in the form of agglomerates, including sinter and pellets. The rational burden structure is an important parameter in strengthening smelting in BF [1]. However, exploring high-quality agglomerates other than sinter and pellets and their rational matching is a final way to really realize the rational burden structure. MgO has long been a flux of focus because it is a significant component in the BF ironmaking process. Many positive comments about the function of MgO flux have been reported in the literature related to traditional BF ironmaking theory [2–3]. However, the behavior of MgO in agglomeration is affected by numerous factors, including the type of ore and the composition of the raw material. For a specific ironmaking system that uses sinter and pellets, the influences of MgO on the production and quality of the sinter or pellets and its suitable content are not the same. Many different conclusions have been reported [4–12].

Yadav *et al.* [4] reported that the addition of MgO reduced the sinter strength by forming glassy dicalcium silicate, which suppressed calcium ferrite formation but improved the softening–melting characteristics. The results reported by Gan *et al.* [5] revealed that the production yield and metallurgical properties of sinter tended to improve with increasing MgO concentration and indicated that an MgO concentration less than 3.7wt% was rational in vanadium-bearing titaniferous magnetite sinter. Dwarapudi *et al.* [6] reported that the addition of MgO in the form of pyroxenite reduced the swelling substantially because of the formation of low-FeO slag that could resist reduction stresses. Moreover, Gao *et al*. [7] presented that when the proportion of light-burned magnesite in pellets was 2.0wt% or less, the compressive strength decreased slightly and the reduction degradation index and reduction swelling index decreased gradually.

The high-chromium vanadium–titanium magnetite (high-chromium VTM) used in the study owning a more complicated chemical composition and mineral phase structure was an important complex mineral resource of high comprehensive utilization value [13–14]. The literature

Corresponding author: Man-sheng Chu E-mail: chums@smm.neu.edu.cn

contains few reports on the effects of MgO flux on agglomeration of this special type of VTM. Therefore, in the present study, the optimized uses of MgO flux in the agglomeration of high-chromium VTM through pellet and sinter experiments were investigated. The effects and mechanism of MgO on the sinter and pellets were investigated systematically by X-ray diffraction (XRD) and scanning electron microscopy (SEM). In addition, the rational BF burden structure for smelting high-chromium VTM was discussed.

2. Experimental

To investigate the optimized use of MgO flux in the agglomeration of high-chromium VTM, the sinter and pellet experiments were conducted separately. In the experiments, MgO was added in the form of magnesite.

2.1. Raw materials

The compositions of the major raw materials used in the sintering tests, including iron ore (high-chromium VTM, iron ore A, iron ore B, and iron ore C), shaft furnace ash, and flux (magnesite and quicklime) are listed in Table 1. The composition of the coke used in the experiments is listed in Table 2. The high-chromium VTM contains some valuable components, such as 0.95wt% V_2O_5, 6.39wt% TiO_2, and 0.47wt% Cr_2O_3.

Table 1. Chemical composition of major sintering materials wt%

Sintering material	TFe	FeO	CaO	SiO_2	MgO	Al_2O_3	TiO_2	V_2O_5	Cr_2O_3
High chromium VTM	61.15	29.11	0.22	2.12	1.07	3.20	6.39	0.95	0.47
Iron ore A	64.50	28.03	0.85	7.00	0.50	0.99	—	—	—
Iron ore B	63.85	27.86	0.05	5.48	0.17	3.66	—	—	—
Iron ore C	61.81	22.21	1.39	3.66	3.54	2.44	—	—	—
Shaft furnace ash	62.56	—	0.31	8.16	0.58	0.92	—	—	—
Magnesite	13.24	5.31	1.05	4.55	35.84	0.97	—	—	—
Quicklime	—	—	70.00	3.69	0.50	—	—	—	—

Table 2. Chemical composition of coke wt%

Fixed carbon	Volatile	Organics	Ash (14.00)						∑
			FeO	CaO	SiO_2	MgO	Al_2O_3	Else	
84.00	0.50	1.50	0.14	0.48	7.50	0.15	2.72	3.01	100.00

In the pellet tests, three types of iron-ore powders (high-chromium VTM, iron ore D, and iron ore E) were used to prepare the high-chromium VTM green pellet; its composition is listed in Table 3. Bentonite was added with a content of 1wt%; its composition is listed in Table 4. As shown in Table 3, the total Fe grade of the high-chromium VTM was lower than those of the other two iron ores.

XRD analysis was used to investigate the phase composition of high-chromium VTM; the results are presented in Fig. 1. Table 5 lists the semi-quantitative analysis results. The high-chromium VTM was composed primarily of magnetite, titanomagnetite, magnesioferrite, chromite, geikielite, and coulsonite. The phase composition of the special iron ore was heterogeneous.

Table 3. Chemical composition of the iron ore used in the pellet tests wt%

Iron ore	TFe	FeO	SiO_2	Al_2O_3	MgO	CaO	P	S	TiO_2	V_2O_5	Cr_2O_3
High chromium VTM	61.15	29.11	2.12	3.20	1.07	0.22	0.02	0.07	6.39	0.95	0.47
Iron ore D	68.32	27.04	5.44	0.32	1.83	0.18	0.02	0.05	—	—	—
Iron ore E	65.02	23.90	8.34	0.05	0.29	0.29	0.00	0.02	—	—	—

Table 4. Chemical composition of the bentonite used in the pellet tests wt%

TFe	FeO	Fe_2O_3	SiO_2	Al_2O_3	CaO	MgO	Na_2O	K_2O
2.00	0.18	2.66	67.45	14.47	2.47	4.61	1.68	1.19

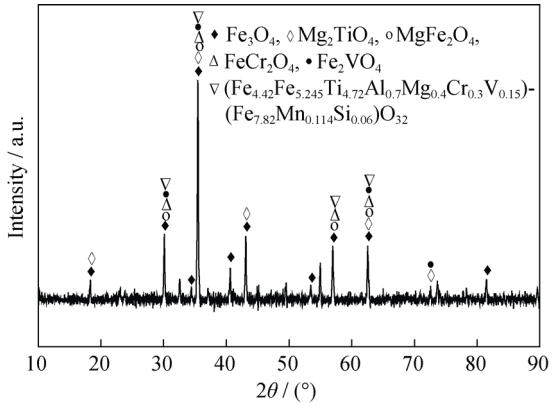

Fig. 1. XRD pattern of high-chromium VTM.

The basic sintering characteristic was a high temperature physical and chemical property of iron ore during the sintering process, which consisted of assimilation temperature, liquid liquidity, binding phase intensity, crystal consolidation strength, etc. In this work, the basic sintering characteristics of the high-chromium VTM were measured; the results are listed in Table 6. This special type of iron ore exhibited a high assimilation temperature (1608 K), a bad liquid liquidity (liquidity index of 1.95), a low grade of binding phase intensity (compression strength less than 450 N), and a bad crystal consolidation strength (compression strength of 365 N).

Table 5. Semi-quantitative analysis results of iron-bearing compounds in the high-chromium VTM

Reference card No.	Name of the chemicals	Chemical formula	Semiquantitative / wt%
01-076-0956	Magnetite	Fe_3O_4	45
01-088-1938	Magnesioferrite	$MgFe_2O_4$	19
01-089-3855	Chromite	$FeCr_2O_4$	17
01-074-2034	Titanomagnetite	$Al_{0.7}Cr_{0.3}Fe_{17.485}Mg_{0.4}Mn_{0.114}O_{32}Si_{0.06}Ti_{4.72}V_{0.15}$	13
01-075-1519	Coulsonite	Fe_2VO_4	5

Table 6. Basic sintering characteristics of the high-chromium VTM

Assimilation temperature / K	Liquidity index	Binding phase intensity / N	Crystal consolidation strength / N
1608	1.95	450	365

In addition, the particle size of three iron ores used to prepare pellets were measured using a laser particle size analyzer (Mastersizer 2000); the results are presented in Table 7. The particle size of the high-chromium VTM was large, and the volume fraction of particles less than 0.074 mm was less than 30vol%. Thus, iron ores D and E with good particle properties were matched during the pelleting process to improve the pelletization properties.

Table 7. Particle size of iron ore powder vol%

Iron ore	High chromium VTM	Iron ore D	Iron ore E
< 0.074 mm	29.98	88.09	83.79

2.2. Experimental scheme and method

According to the requirements for practical production, the basicity of the high-chromium VTM sinter was maintained at 2.25. By changing the additive amount of magnesite, the content of MgO in the sinter was adjusted to 1.95wt%, 2.10wt%, 2.25wt%, 2.40wt%, and 2.63wt%, separately; the detailed scheme is given in Table 8. As shown in Fig. 2, a ϕ150-mm sinter pot system designed by Northeastern University was used in the sintering tests; the efficient efficient height of the system was 535 mm. The whole sintering test comprised several steps, including mixing and pelletizing, charging, opening the fan, performing shatter and tumbler tests, etc. The pelletizing time was 10 min, the moisture was 8.8wt% ± 0.3wt%, the hearth layer for sinter was 30 mm, the ignition negative pressure and convulsion negative pressure were controlled at 5.0 and 10.0 kPa, respectively, and the ignition temperature was 1273 K. The shattering, screening, and tumbler indices were tested in accordance with standard ISO3271. In addition, on the basis of GB/T13241—91, the reduction disintegration index (RDI) of the high-chromium VTM sinter with different MgO contents was measured using the equipment shown in Fig. 3.

In the pellet tests, the content of MgO in the high-chromium VTM pellets was adjusted to 1.14wt%, 1.50wt%, 1.80wt%, 2.10wt%, and 2.40wt%, respectively. The detailed scheme is given in Table 9. The pellet test consisted of several steps, including batching, mixing, pelletizing, drying, and roasting. The high-chromium VTM green pellet samples were prepared using a disc pelletizer that produces discs with a diameter of 1000 mm; the rotation speed of the pelletizer was 18 r/min, and its dip angle could be adjusted from 45° to 47°. Preheating and roasting were performed in a muffle furnace, and the roasting temperature and time were 1473 K and 20 min, respectively. The metallurgical properties, including the compressive strength (CS) of the oxidized pellet and the reduction swelling index (RSI), were subsequently measured.

Table 8. Burdening scheme of the high-chromium VTM sinter wt%

No.	High chromium VTM	Iron ore A	Iron ore B	Iron ore C	RM	SFA	Magnesite	Quicklime	Coke
S-1.95	13.44	15.53	20.67	12.41	14.00	4.50	2.00	12.45	5.00
S-2.10	13.37	15.45	20.55	12.35	14.00	4.50	2.33	12.45	5.00
S-2.25	13.30	15.35	20.44	12.28	14.00	4.50	3.02	12.40	5.00
S-2.40	13.23	15.28	20.35	12.22	14.00	4.50	3.02	12.40	5.00
S-2.63	13.11	15.12	20.18	12.12	14.00	4.50	3.57	12.40	5.00

Note: RM—Return mine; SFA—Shaft furnace ash.

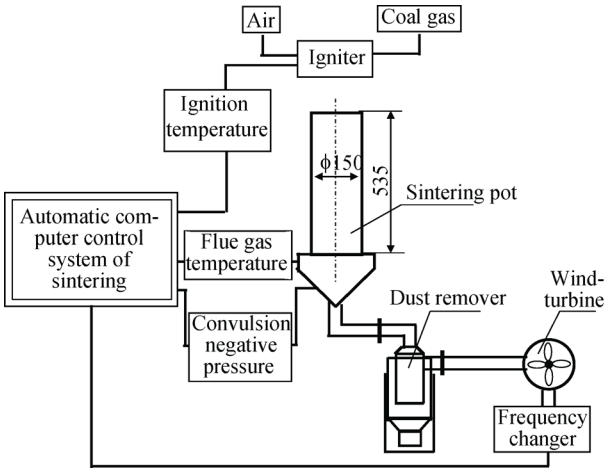

Fig. 2. Sketch of the sinter pot system.

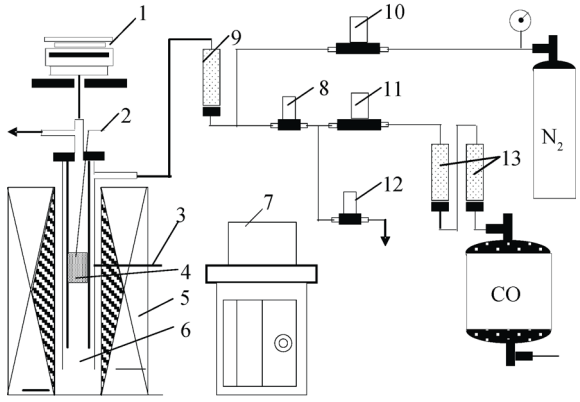

1—Electronic scales; 2,3—Thermocouple; 4—Sample; 5—Electric furnace; 6—Reduction tube; 7—Computer measure and control system; 8—Cut-off solenoid valve; 9,13—Silica gel; 10,11—Mass flowmeter; 12—Blow-off solenoid valve

Fig. 3. Equipment used in low-temperature reduction disintegration.

Table 9. Burdening scheme of the high-chromium VTM pellets wt%

No.	High chromium VTM	Iron ore D	Iron ore E	Bentonite (additional)	Magnesite (additional)
P-1.14	45	35	20	1.0	0
P-1.50	45	35	20	1.0	1.0
P-1.80	45	35	20	1.0	1.8
P-2.10	45	35	20	1.0	2.6
P-2.40	45	35	20	1.0	3.4

3. Results and discussion

3.1. Effects of MgO flux on the high-chromium VTM sinter

3.1.1. Effects of MgO flux on the high-chromium VTM sintering process indices

The vertical sintering speed, yield, utilization coefficient, and tumbler index were the key indices in the sintering process. In addition, to obtain a comprehensive evaluation of the sintering, a comprehensive index was used, given as "(yield × 40%) × (tumbler index × 30%) × (utilization coefficient × 30%)" [15]. The effects of MgO flux on the sintering process indices and on the cold strength of the high-chromium VTM sinter were evaluated on the basis of the results summarized in Tables 10 and 11, respectively.

(1) Sintering speed. With increasing MgO content, the vertical sintering speed of the high-chromium VTM sinter decreased slightly. When the MgO content was increased from 1.95wt% to 2.63wt%, the vertical sintering speed

Table 10. Effects of MgO content on the sintering process indices

No.	Vertical sintering speed / (mm·min^{-1})	Yield / %	Utilization coefficient / (t·m^{-2}·h^{-1})	Tumbler index / %	Comprehensive index*
S-1.95	26.96	68.77	1.71	50.53	213.50
S-2.10	24.44	70.79	1.61	52.22	214.72
S-2.25	24.72	70.31	1.66	51.59	216.26
S-2.40	23.45	73.23	1.61	53.32	226.48
S-2.63	23.68	74.18	1.74	53.40	248.13

Note: * Comprehensive index = (yield × 40%) × (tumbler index × 30%) × (utilization coefficient × 30%).

Table 11. Effects of MgO flux on the cold strength of the high-chromium VTM sinter

No.	Drop size distribution				Tumbler strength	
	w_{5-10} / %	w_{10-25} / %	w_{25-40} / %	$w_{>40}$ / %	$w_{+6.3}$ / %	$w_{-0.5}$ / %
S-1.95	12.80	38.15	9.79	9.16	50.53	3.82
S-2.10	14.67	36.10	8.07	13.00	52.22	4.67
S-2.25	16.81	35.56	7.03	11.95	51.59	3.97
S-2.40	14.54	37.12	11.44	11.09	53.32	5.72
S-2.63	16.26	36.85	10.14	11.81	53.40	4.48

Note: w_{5-10}, w_{10-25}, w_{25-40}, $w_{>40}$, $w_{+6.3}$, and $w_{-0.5}$ are the mass fractions of the sinters with the particle sizes of 5–10, 10–25, 25–40, >40, >6.3, and <0.5 mm, respectively.

decreased from 26.96% to 23.68% accordingly (Fig. 4). This decrease was primarily a consequence of the large size, small specific surface area, poor hydrophobicity, and poor caking of the magnesite used to adjust the content of MgO. As a result, both the mixing and pelleting became worse, the air permeability of the burden decreased, the resistant loss of the burden increased, and the heat transfer condition deteriorated. All of these effects could result in a decrease in the vertical sintering speed of the high-chromium VTM sinter [16–17].

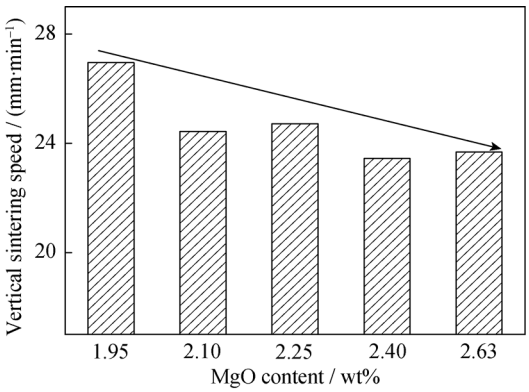

Fig. 4. Effect of MgO content on the vertical sintering speed of the high-chromium VTM sinter.

(2) Yield and strength of sinter. With increasing MgO flux content, the yield and strength of the high-chromium VTM sinter tended to improve. As the MgO content was increased from 1.95wt% to 2.63wt%, the yield gradually improved from 68.77% to 74.18% (Fig. 5). This improvement was possibly due to the increased amounts of minerals titanomagnetite, forsterite, and pyroxene and the decreased amount of vitric with increasing MgO content. The structure of the minerals tended to become gradually more complicated. All of these factors could lead to an improvement in the cold strength of the high-chromium VTM sinter [8]. In addition, the sintering speed obviously slowed and the maintained time of the high-temperature segment was prolonged with increasing MgO content, which contributed to the development of the liquid phase and led to better concretion and cold strength of the high-chromium VTM sinter [18].

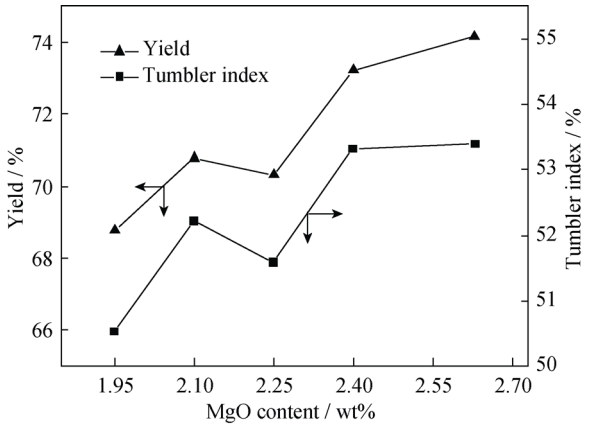

Fig. 5. Effect of MgO content on the yield and tumbler index of the high-chromium VTM sinter.

To further elucidate the effects of MgO flux on the strength of the high-chromium VTM sinter, we observed the sinters with MgO contents of 2.25wt% and 2.63wt% by SEM (Fig. 6). Four types of mineral phase structures, given as points a, b, c, and d in Fig. 6, were observed. Among them, phase a was iron oxide with small amounts of Ca, Si, Mg, and Al. Phase b was mainly composed of Fe, Ca, Si, Al, and O. In addition, on the basis of the EDS analysis results and the mineral composition and structure, phase b was judged to be the acicular composite calcium ferrite (a solid solution of $CaO{\cdot}SiO_2$–$CaO{\cdot}3(Fe,Al)_2O_3$, abbreviated as SFCA), which was the dominant binding phase of the sinter [13]. Phase c was calcium ferrite and ilmenite. Phase d was calcium silicate.

When the MgO content in the high-chromium VTM sinter was 2.25wt%, the SFCA was acicular and sparse, as shown in Fig. 6(a). When the MgO content was 2.63wt%, the SFCA was bar-shaped and the crystal was bulky and dense, as shown in Fig. 6(b). The sinter was usually composed of some minerals, and each mineral exhibited a prop-

erty referred to essence strength, which allowed each mineral to bear a certain pressure. The bar-shaped SFCA exhibited high essence strength for its compact structure. As the MgO content was increased, more bar SFCA formed, and the strength of the high-chromium VTM sinter was therefore enhanced. In addition, when the MgO content was 2.25wt%, the silicate (phase d) formed some independent phases and the single grains were not bonded with other minerals, as shown in Fig. 6(a). When the MgO content was 2.63wt%, the silicate was disseminated in the gaps of other minerals, with good bonding; the strength of the sinter with relatively compact and strong microstructure consequently increased. Moreover, in the sinter with 2.63% MgO, the porosities exhibited a good fractal structure and an evenly distributed size, which both provided further explanations for the improved strength with increasing MgO content.

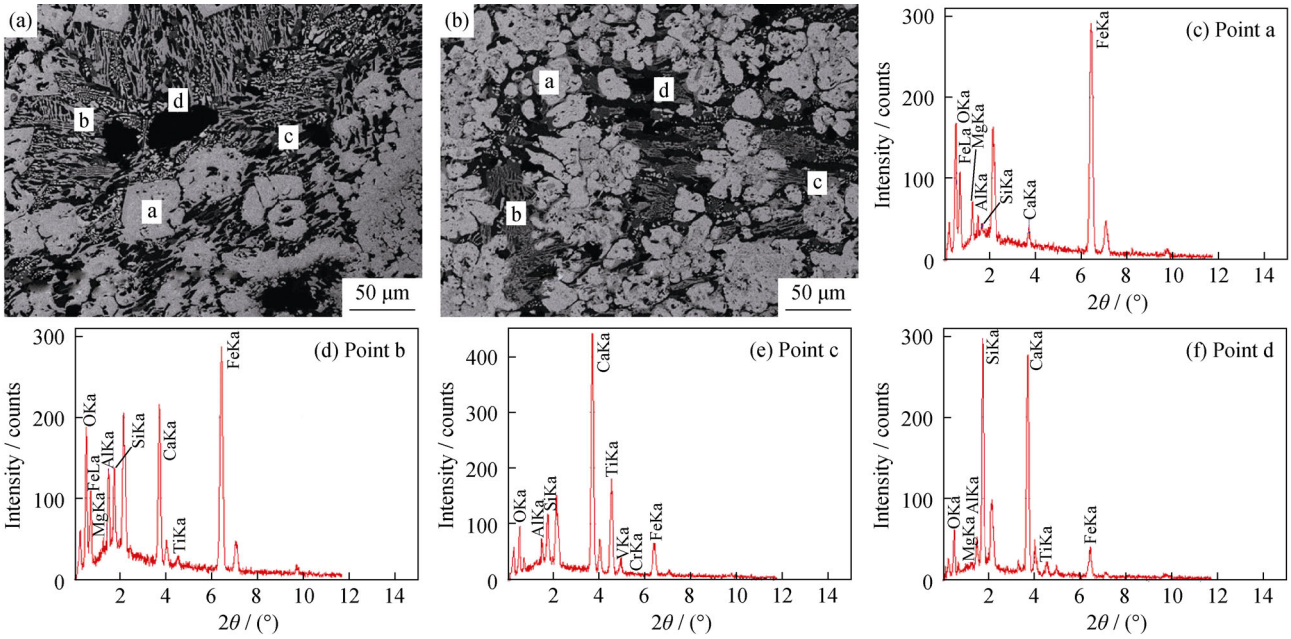

Fig. 6. SEM images of high-chromium VTM sinters S-2.25 (a) and S-2.63 (b); EDS spectra of points a (c), b (d), c (e), and d (f).

Sintering of a good solid-phase concretion was another important way to improve the quality of the sinter. Because the high-chromium VTM sinter was a heterogeneous body, solid concretions were present only in some small regions. Through high temperature sintering, the solids, including Fe_2O_3 and Fe_3O_4, were formed during cooling. As shown in Fig. 6(a), the dispersed iron oxides (phase a) in the sinter with 2.25wt% MgO were single and angular grains. However, as shown in Fig. 6(b), the iron oxides in the sinter with 2.63wt% MgO were well developed; the grains were large and linked end-to-end, and the concretion was good. As a result, the strength of the high-chromium VTM sinter gradually improved with increasing content of MgO, resulting in the excellent structure of iron oxide [16].

(3) Utilization coefficient and comprehensive index. In the MgO content range investigated in the experiments, the utilization coefficient did not obviously change: it remained approximately 1.71 $t \cdot m^{-2} \cdot h^{-1}$ as the MgO content in the high-chromium VTM sinter was increased (Fig. 7). The reasons for the relatively constant utilization coefficient were deduced from the decreased vertical sintering speed and increased yield and strength. In addition, when the MgO content was increased from 1.95wt% to 2.63wt%, the comprehensive index of the high-chromium VTM sinter improved from 213.50 to 248.13 (Fig. 7) and the sintering process was accordingly enhanced.

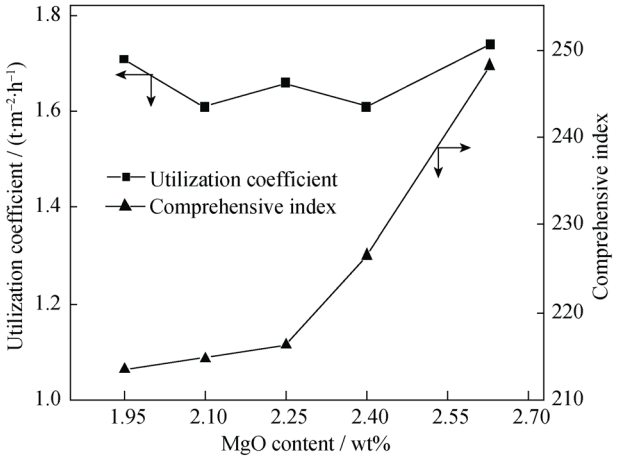

Fig. 7. Effect of MgO content on the utilization coefficient and comprehensive index of the high-chromium VTM sinter.

3.1.2. Effects of MgO flux on the RDI of the high-chromium VTM sinter

The effects of MgO flux content on the RDI of the high-chromium VTM sinter are given in Table 12. The RDI increased with increasing MgO content. Two factors are responsible for the increased RDI. First, the rhombic titanohematite in the high-chromium VTM sinter underwent a volume expansion and fragmentation during the phase change. Moreover, the fracture of titanohematite was also observably destroyed by the TiO_2 and Al_2O_3 dissolved in the silicates of the glass phase and in the schorlomite. In the accumulation area of the schorlomite, especially in the case of large schorlomite particles, some coarse cracks were expanded ulteriorly by the function of stress during the reduction process. Thus, the high-chromium VTM sinter was degraded. In addition, with increasing MgO content, the solid solution generated from MgO and titanomagnetite was dispersed in the high-chromium VTM sinter, which restrained the oxidation from Fe_3O_4 to Fe_2O_3. Less rhombic coarse titanohematite was generated, and the sinter with micropores and thick walls was produced. The strength of the high-chromium VTM sinter was consequently increased [8]. In addition, the crystallization capacity of the silicate melts was improved, and the amount of glass phase was decreased as a result of the function of MgO flux. Some forsterite and pyroxene, which acted as the skeleton, were separated from the glass phase. The ability of the high-chromium VTM sinter to resist the variation of stresses and crack growth was enhanced, and the RDI of the high chromium VTM sinter was improved.

Table 12. Effects of MgO content on the RDI of the high-chromium VTM sinter

No.	m_{D0} / g	$m_{+6.3}$ / g	$m_{3.15-6.3}$ / g	$m_{-0.5}$ / g	$RDI_{+6.3}$ / wt%	$RDI_{+3.15}$ / wt%	$RDI_{-0.5}$ / wt%
S-1.95	500.00	305.04	97.83	18.13	61.01	80.57	3.63
S-2.10	499.68	319.43	84.57	25.21	63.93	80.85	5.05
S-2.25	499.47	328.80	80.36	21.06	65.83	81.92	4.22
S-2.40	498.29	328.82	78.76	17.75	66.79	82.60	3.56
S-2.63	499.20	337.24	75.66	18.76	67.56	82.71	3.76

Note: m_{D0}—initial mass; $m_{+6.3}$, $m_{3.15-6.3}$, $m_{-0.5}$—mass of the sinter with the particle sizes of >6.3, 3.15–6.3, and <0.5 mm, respectively; $RDI_{+6.3}= m_{+6.3}/m_{D0}\times100\%$; $RDI_{+3.15}= (m_{+6.3.}+ m_{3.15-6.3})/m_{D0}\times100\%$; $RDI_{-0.5}= m_{-0.5}/m_{D0}\times100\%$.

In contrast, during the process of cooling, transformation from β-C_2S to γ-C_2S could lead to an increase in volume and render the high-chromium VTM sinter easy to degrade. However, the partial dissolution of Mg^{2+} into the lattice of β-C_2S could suppress the phase change from β-C_2S to γ-C_2S. As a consequence, the amount of γ-C_2S produced decreased, and the RDI of the high-chromium VTM sinter increased.

On the basis of all of the above analyses of the high-chromium VTM sinter, the metallurgical properties were improved with increasing MgO content. Among the investigated concentrations of MgO in the high-chromium VTM sinter, the concentration of 2.63wt% is recommended.

3.2. Effects of MgO flux on the high-chromium VTM oxidized pellet

3.2.1. Effects of MgO flux on the properties of the high-chromium VTM green pellet

The properties of the high-chromium VTM green pellet with different MgO contents were investigated. As shown in Table 13, with increasing MgO content, the drop strength did not obviously change, but the compressive strength increased slightly. In general, no significant changes in the properties of the high-chromium VTM green pellet were observed.

Table 13. Properties of the high-chromium VTM green pellet

No.	Drop strength / time	Compressive strength / N	Moisture / wt%
P-1.14	3.3	16.7	8.3
P-1.50	3.2	16.5	7.7
P-1.80	3.4	16.8	8.5
P-2.10	3.3	17.1	8.1
P-2.40	3.4	17.3	8.2

3.2.2. Effects of MgO flux on the CS of the high-chromium VTM oxidized pellet

The effects of the MgO flux on the CS of the high-chromium VTM oxidized pellet are indicated in Fig. 8. As evident in the figure, when the content of MgO was increased, the CS tended to decrease inversely from 1985 N to 1479 N; this lower CS does not satisfy the requirement for BF pro-

duction.

In the case of the same roasting conditions and similar particle sizes of mixed materials, the decrease in CS was usually caused by variations in the chemical composition, especially the MgO content. In the roasting process, the CS was controlled and determined by the microstructure of the oxidized pellet. To further analyze these effects, high-chromium VTM oxidized pellets with 1.14wt% and 2.40wt% MgO were investigated. As shown in Fig. 9, phase a was iron oxide and phase b was mainly the slag. When the content of MgO in the high-chromium VTM oxidized pellet was 1.14wt%, the iron mineral was epigranular, the slag was scattered and disseminated, and the pellet exhibited good concretion (Fig. 9(a)). When the content of MgO was increased to 2.40wt%, the iron mineral particles of different sizes and the centralized distribution of the slag obviously led to a diminished CS of the high-chromium VTM oxidized pellet (Fig. 9(b)).

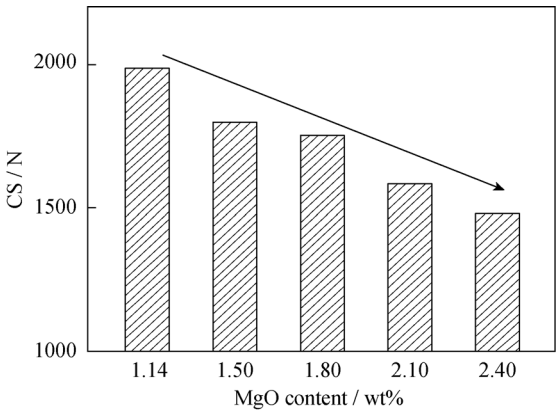

Fig. 8. Effect of MgO content on the compressive strength (CS) of the high-chromium VTM oxidized pellets.

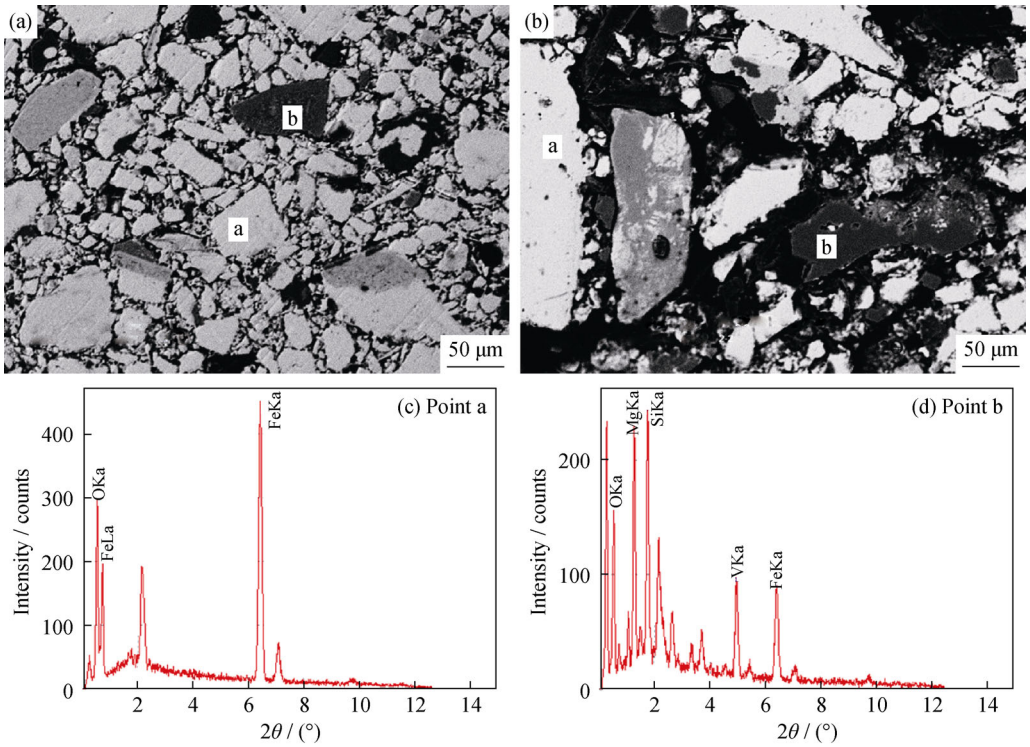

Fig. 9. SEM micrographs and EDS spectra of the high-chromium VTM oxidized pellets (P-1.14 and P-2.40).

Moreover, the particles were primarily bonded by the solid concretion of recrystallized Fe_3O_4 during the roasting process of the high-chromium VTM oxidized pellet. After MgO was added, Mg^{2+} diffused into the lattice of Fe_3O_4 and prevented it from oxidizing, which inhibited both the formation of Fe_2O_3 and recrystallization. At a roasting temperature of 1473 K, the CS decreased if the MgO did not fully mineralize and entered into the slag. In addition, when more MgO was added, the mineral particles in the high-chromium VTM oxidized pellet were isolated from each other, which hindered the bonding function of the crystallization and growth of the primary hematite, which, in turn, resulted in decreased CS under the same roasting temperature [19–20].

3.2.3. Effects of MgO flux on the RSI of the high-chromium VTM oxidized pellet

The reduction swelling index (RSI) of the high-chromium VTM oxidized pellet was determined; the results are presented in Fig. 10. The RSI clearly improved with the increasing MgO content. When the MgO content in the oxidized pellet was increased from 1.14wt% to 2.40wt%, the

RSI decreased from 15.2% to 8.6% accordingly. These results indicated that an appropriate MgO content in the high-chromium VTM oxidized pellet could enhance the reduction swelling property, which would be beneficial to normal BF production.

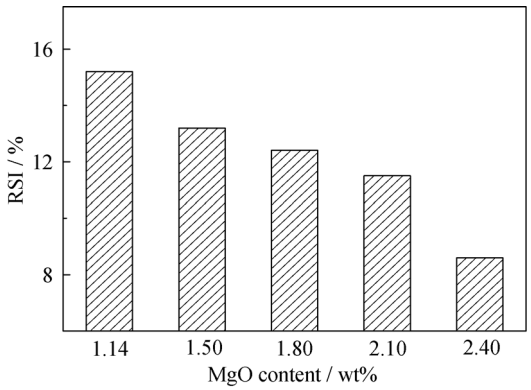

Fig. 10. Effect of MgO content on the reduction swelling index (RSI) of the high-chromium VTM oxidized pellets.

The XRD pattern of the high-chromium VTM oxidized pellet with 1.14wt% MgO is shown in Fig. 11. The binary phase diagram of MgO–Fe_2O_3, which was drawn using the Factsage 6.4 software, is shown in Fig. 12. As evident in Fig. 12, a region marked with a red dashed line existed where the roasting was complete. Figs. 11 and 12 indicate that Mg^{2+} and Fe^{2+} could partially substitute each other and that stable magnesium ferrite (MgO·Fe_2O_3) was generated during the roasting process, which could restrain the transformation from Fe_2O_3 to Fe_3O_4 during the reduction of the high-chromium VTM oxidized pellet. In addition, a solid solution of FeO and MgO was produced during the medium-temperature reduction, which could prevent the generation of iron whiskers and restrain the swelling of the high-chromium VTM oxidized pellet.

Because the radius of Mg^{2+} is less than that of Fe^{2+} (0.74×10^{-10} m) and Ca^{2+} (0.99×10^{-10} m), the Mg^{2+} can equally distribute in Fe_xO without inducing partial stress. The structure and holes in the pellet after reduction were distributed uniformly. The degradation and swelling of high-chromium VTM oxidized pellet consequently decreased.

The ternary phase diagram of FeO–MgO–SiO_2 drawn using the Factsage 6.4 software is shown in Fig. 13. According to the phase diagram, the formed low-FeO slag can resist reduction stresses. In addition, the increasing MgO content in the high-chromium VTM oxidized pellet could significantly increase the melting temperature of slags, which would produce sufficient bonding strength to restrain the swelling behaviors.

The experiments on the high-chromium VTM oxidized pellet indicated that the pellets with low MgO contents should be used in the smelting of high-chromium VTM in BFs. However, the compressive strength of the pellet with 1.14wt% MgO does not satisfy the requirements for BF production. Therefore, the MgO content in high-chromium VTM oxidized pellets should be less than 1.14wt%.

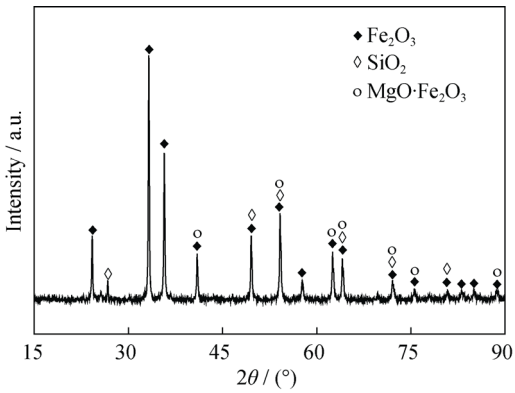

Fig. 11. XRD pattern of the high-chromium VTM oxidized pellet with 1.14wt% MgO.

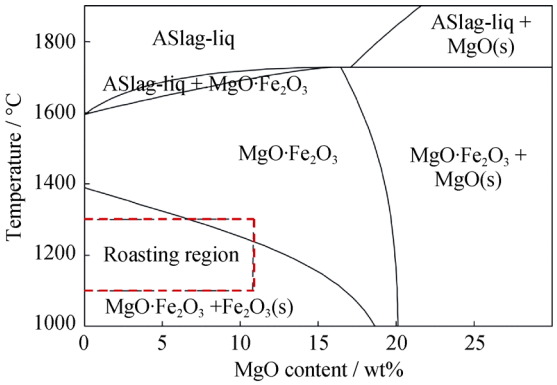

Fig. 12. Binary phase diagram of MgO–Fe_2O_3.

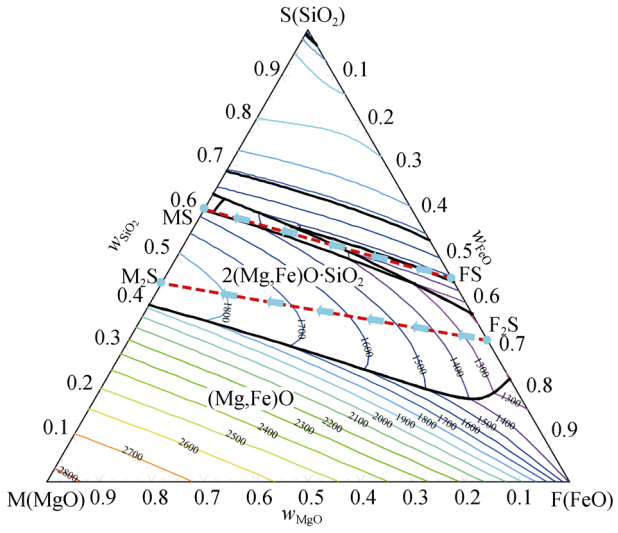

Fig. 13. Ternary phase diagram of FeO–MgO–SiO_2 (temperature, °C).

4. Conclusions

(1) High-chromium VTM with a large particle size is mainly composed of magnetite, titanomagnetite, magnesioferrite, chromite, geikielite, and coulsonite. It exhibits a high assimilation temperature (1608 K), a bad liquid liquidity (liquidity index of 1.95), a low grade of binding phase intensity (compression strength less than 450 N), and a bad crystal consolidation strength (compression strength of 365 N).

(2) When the MgO content in the high-chromium VTM sinter is increased from 1.95wt% to 2.63wt%, the low-temperature reduction degradation index increases from 80.57% to 82.71%. The other indices are all satisfactory under the experimental conditions used in this work.

(3) When the MgO content in the high-chromium VTM oxidized pellet is increased from 1.14wt% to 2.40wt%, the reduction swelling index dramatically decreases from 15.2% to 8.6%. However, when the MgO content is 1.14wt%, the CS of the high-chromium VTM pellet is 1985 N, which does not satisfy the requirements for BF production.

(4) In the investigated experimental range of MgO contents, the sinter with the highest MgO (2.63wt%) content that matches the pellet with the low MgO content (less than 1.14wt%) is the rational burden structure for smelting high-chromium VTM in a BF. Optimized use of MgO flux in the agglomeration of high-chromium VTM is achieved.

Acknowledgements

This work was financially supported by the National Natural Science Foundation of China (Major Program, No. 51090384), the National High Technology Research and Development Program of China (Nos. 2012AA062302 and 2012AA062304), the Fundamental Research Funds for Central Universities (Nos. N110202001 and N130602003), and the Northeastern University Cultivation Project of Excellent Doctoral Dissertation.

References

[1] M.Y. Zhu, *Modern Metallurgy* (*Metallurgy of Iron and Steel*), Metallurgical Industry Press, Beijing, 2008.

[2] X.L. Wang, *Iron and Steel Metallurgy*, Metallurgical Industry Press, Beijing, 2002.

[3] S.L. Wu, H.L. Han, W.Z. Jiang, J.M. Zhu, G.S. Feng, and Z.C. Zhang, MgO interaction mechanism in sinter, *J. Univ. Sci. Technol. Beijing*, 31(2009), No. 4, p. 428.

[4] U.S. Yadav, B.D. Pandey, B.K. Das, and D.N. Jena, Influence of magnesia on sintering characteristics of iron ore, *Ironmaking Steelmaking*, 29(2002), No. 2, p. 91.

[5] Q. Gan, Q. He, and Y.C. Wen, Study on Influence of MgO on mineral composition and metallurgical properties of V-bearing titaniferous magnetite sinter, *Iron Steel*, 43(2008), No. 8, p. 7.

[6] S. Dwarapudi, T.K. Ghosh, A. Shankar, V. Tathavadkar, D. Bhattacharjiee, and R. Venugopal, Effect of pyroxenite flux on the quality and microstructure of hematite pellets, *Int. J. Miner. Process.*, 96(2010), No. 1-4, p. 45.

[7] Q.J. Gao, F.M. Shen, G. Wei, X. Jiang, and H.Y. Zheng, Effects of MgO containing additive on low-temperature metallurgical properties of oxidized pellet, *J. Iron Steel Res. Int*., 20(2013), No. 7, p. 25.

[8] Q. Gan, Q. He, and Y.C. Wen, Influence of MgO content on productivity and quality of V-bearing titaniferous magnetite sinter, *Iron Steel Vanadium Titanium*, 29(2008), No. 1, p. 54.

[9] X.H. Fan, Q.W. Li, M. Gan, X.L. Chen, L.S. Yuan, and Z.Y. Ji, Influence and mechanism of MgO on strength of high basicity sinter, *J. Cent. South Univ. Sci. Technol.*, 43(2012), p. 3325.

[10] K. Higuchi, M. Naito, M. Nakano, and Y. Takamoto, Optimization of chemical composition and microstructure of iron ore sinter for low-temperature drip of molten iron with high permeability, *ISIJ Int.*, 44(2004), No. 12, p. 2057.

[11] M. Nakano, M. Naito, K. Higuchi, and K. Morimoto, Non-spherical carbon composite agglomerates: lab-scale manufacture and quality assessment, *ISIJ Int*., 44(2004), No. 12, p. 2079.

[12] H. Kimura, T. Ogawa, M. Kakiki, A. Matsumoto, and F. Tsukihashi, Effect of Al_2O_3 and MgO additions on liquidus for the CaO–SiO_2–FeO_x system at 1573 K, *ISIJ Int.*, 45(2005), No. 4, p. 506.

[13] J. Tang, Y. Zhang, M.S. Chu, and X.X. Xue, Preparation of oxidized pellets with high chromium vanadium–titanium magnetite, *J. Northeast. Univ. Nat. Sci.*, 34(2013), No. 4, p. 545.

[14] J. Tang, Y. Zhang, M.S. Chu, and X.X. Xue, Effect of the increasing percent of high chromium vanadium-titanium magnetite on quality of oxidized pellets, *J. Northeast Univ. Nat. Sci.*, 34(2013), No. 7, p. 956.

[15] Ironmaking plant of Pangang Group Panzhih Steel & Vanadium, *Pangang Group Vanadium Titanium, Technological Paper Assembly of Strengthening Smelting Vanadium–titanium Magnetite in Large-scale Blast Furnace for Panzhihua Iron & Steel*, 2000-2010, p. 626 and 632.

[16] Y. M. Chen and R. Chen, *Microstructure of Sinter and Pellet*, Central South University Press, Changsha, 2002.

[17] M. Matsumura, M. Hoshi, and T. Kawaguchi, Improvement of sinter softening property and reducibility by controlling chemical compositions, *ISIJ Int.*, 45(2005), No. 4, p. 594.

[18] G.F. Zhou and F. Yang, Effects of adding MgO on pelletizing ability and strength of pellet, *Res. Iron Steel*, 37(2009), No. 2, p. 10.

[19] S. Dwarapudi and M. Ranjan, Influence of oxide and silicate melt phases on the RDI of iron ore pellets suitable for shaft furnace of direct reduction process, *ISIJ Int.*, 50(2010), No. 11, p.1581.

[20] X.H. Fan, M. Gan, T. Jiang, X. Chen, and L. Yuan, Influences of MgO on roasting properties of oxidized iron ore pellets, [in] *The* 2010 *TMS Annual Meeting & Exhibition,* Warrendale, 2010, p. 559.